Interface Engineering in hybrid Quantum Dot – 2D phototransistors

Dominik Kufer[1], Tania Lasanta[1], Maria Bernechea[1], Frank Koppens[1,2] and Gerasimos Konstantatos[1,2,]*

[1]ICFO – Institut de Ciencies Fotoniques, The Barcelona Institute of Science and Technology, Castelldefels, 08860, Barcelona, Spain

[2]ICREA-Institució Catalana de Recerca i Estudis Avançats, Lluis Companys 23, 08010 Barcelona, Spain

E-mail: (Gerasimos.konstantatos@icfo.es)
Keywords: (MoS_2, TiO_2, PbS, photodetector, passivation, gain)

The hybridization of two-dimensional transition metal dichalcogenides (TMDCs) with colloidal quantum dots has been demonstrated to be an ideal platform for low dark-current and highly sensitive photodetection due to a carrier recirculation mechanism producing very high gain. However, TMDCs react sensitively to surface modifications and the sensitizing quantum dots introduce uncontrolled doping, which prevent these hybrids from reaching large on/off ratios, met in pristine 2D transistors. In this work, we report on a new hybrid device architecture with a semiconducting TiO_2 buffer layer at the interface of molybdenum disulfide (MoS_2) and lead sulfide (PbS) QDs. The buffer layer encapsulates the MoS_2 transistor and preserves the gate modulation by suppressing the high density of localized sub-bandgap states that pin the Fermi level. The maintained gate control over carrier density in the conduction channel allows for low noise operation similar to pristine MoS_2 devices. We report on effective charge transfer with quantum efficiency of 28%, a photoconductive gain that can be tuned with gate voltage yielding responsivity of 10^3–10^5 A/W, and specific detectivity of 5×10^{12} Jones, an improvement of more than one order of magnitude compared to MoS_2/PbS

devices without buffer layer. The present methodology discloses a new path to control interface and degenerate doping effects of 2D-crystal-based hybrid devices.

In modern optoelectronics the p-n-junction is at the heart of a vast range of device building blocks. In photodiodes, for instance, the high electric field within the depleted p-n-interface region serves to separate electron-hole pairs after photoexcitation and forms the basis of sensitive photodetection. Apart from photodiodes, the p-n-junction can also be beneficial for phototransistors, where the decoration of the channel material with semiconductors of opposite doping polarity creates interesting new device designs with improved light response. Especially in the case of ultrathin two-dimensional channel materials such as the TMDCs or graphene[1], this sensitizing approach enhances the inherently low absorption of 2D materials, owing to its atomic thickness. Graphene has been sensitized with a multitude of absorbing semiconductors such as CQDs[2,3], TiO_2[4], perovskites[5] or other 2D materials[6,7], leading to reported responsivities as high as 10^5–10^{10} A/W, where typically the highest responsivity values are followed by impractically slow photoresponse. The lack of bandgap and its corresponding high noise current and power consumption, however, impose challenges for its application in low power electronics. Recently, phototransistors based on MoS_2 have drawn substantial attention, as their bandgap allows gate-controllable operation at low off-currents[8–12]. When employed as the conducting channel in hybrid phototransistors, the reported mobility of MoS_2, in the range of 1–60 cm^2/Vs, is beneficial when hybridizing it with low mobility material systems such as QDs (10^{-3} cm^2/Vs). A considerably high gain of 10^6 electrons per absorbed photon along with decay times in the range of 300–400 ms were reported in first MoS_2/PbS hybrids[13]. However, despite its large bandgap of 1.2–1.8 eV, the initially high on/off ratio decreases significantly upon sensitization with QDs resulting in

large dark currents of 10–100 nA, several orders of magnitude above those reported in pristine MoS_2 transistors.

The atomically thin profile renders TMDCs extremely sensitive to surface modifications. Controlled doping strategies still remain poorly understood and form one of the key challenges in 2D-based optoelectronics. Various different approaches based on molecular doping[14–18], substitutional doping[19,20], chemical surface treatment[21,22] or strong bonding to defect sites[23,24] have been employed. However, most of them yield either in degenerate doping with metallic behaviour or strongly reduced electrical gate-modulation, as in the case of MoS_2/PbS. While degenerate doping is useful for high quality contact formation with reduced contact resistance[16], the loss of on/off ratio is detrimental for high sensitivity photodetectors. Recently, it was found that defect sites, such as sulphur vacancies, play a major role in MoS_2 doping, as they offer connecting links for organic functional groups[24]. In optoelectronic heterojunctions, this can lead to a fundamental trade-off: for one, hybrids rely on strong electrical coupling at the interface for efficient charge transfer. For this purpose, defect sites can be useful to adhere organic functional groups and crosslink the sensitizers. However, the direct crosslinking of sensitizers at defects may also lead to aforementioned uncontrolled doping effects, increased charge scattering or a high density of localized states, which affect the electrical modulation efficiency and charge transport of the hybrid. A new path has to be found to combine TMDCs with sensitizers to form efficient heterojunctions and support charge transfer without compromising its unique electronic transport properties.

In this letter we implement interface engineering by using an appropriate buffer layer between MoS_2 sheets and colloidal QDs to maintain the FET characteristics of the MoS_2 channel and thereby improve phototransistor performance. We chose the large bandgap semiconductor TiO_2, as its energy levels align well at the MoS_2/PbS interface to form an

efficient p-n-junction with PbS and facilitate electron transfer to the MoS_2 channel. It simultaneously passivates the interface region and suppresses high density of localized states. The latter are responsible for Fermi-level pinning and reduction of the modulation capacity of the phototransistor. We compare the new device design to MoS_2/PbS control devices and demonstrate an improvement in on/off ratio by more than 2 orders of magnitude, high sensitivity of 5×10^{12} Jones in the visible and fast response times of less than 12 ms. This new approach paves the way for a wide range of hybrid optoelectronic devices based on 2D crystals, where the control of interface and doping is of major importance.

Results

Preparation and device architecture. We began our study by fabricating standard MoS_2 field effect transistors with a variety of channel thickness from 1 to 10 layers. The flakes were exfoliated by using PDMS tape, a method described recently by Li et al.[25] to achieve larger device dimensions, which in our case range from 30–50 μm^2. Figure 1a shows a sequence of device fabrication steps from left to right, which includes standard MoS_2 FET fabrication with Ti/Au metal contacts, ALD deposition of a thin buffer oxide layer, and a final spincoating deposition of the QD film. As shown in previous work, the encapsulation with isolating oxides as HfO_2 or Al_2O_3 in a high temperature process enhanced electronic performance by boosting mobility, reducing hysteresis, and increasing device on-currents[9]. In this work, we chose the semiconducting oxide TiO_2 over the previously reported insulating oxide films. The semiconducting character of this interlayer is important for it not only serves as a protection layer, but also acts as an efficient electron transport medium between MoS_2 and PbS. TiO_2 is a well-studied n-type semiconductor, often used in solar cells to form an effective p-n-junction with colloidal PbS quantum dot films[26–28]. The large bandgap of 3.2 eV further ensures that TiO_2 has no impact on the optical properties of the device in the vis/NIR

as its absorption is limited to UV radiation. The thickness of the TiO_2 film was tested from 5–40 nm, but had no clear influence in this range on final photodetecting device performance or on/off ratio (see SOM T1). All devices reported in this manuscript possess therefore a standard thickness of 25 nm. In a last step of the fabrication process, the PbS quantum dots were spincoated from solution in a layer-by-layer technique up to a thickness of 80–100 nm. More details on device fabrication can be found in the methods section and supplementary information.

Transport properties of hybrid stages. To evaluate the electrical performance of the new device design, we investigated the transfer curve I_{DS}-V_G. Figure 1b and c summarize the modulation curves of a 5-layer MoS_2 device after each fabrication step, measured under bias voltage of 1V. From previous results we know that encapsulation with oxides can lead to n-type doping effects due to removal of adsorbates or due to oxygen vacancies in non-stoichiometric oxide films, that create donor states close to the conduction band[9]. We found a similar electron doping effect upon encapsulation with ALD deposited TiO_2 as compared to other oxides. Although the ALD deposited material is in contact with the Au source- and drain-electrode, the low mobility of the non- stoichiometric TiOx and a non-ohmic alignment to contacts lead to negligible current leakage through the oxide film. The previous MoS_2-FET characteristics are mostly maintained and typically off-currents of 100 pA are reached. The increase in off-current was found to be independent on TiO_2 thickness up to 40 nm, suggesting that the off-current doesn`t stem from leakage through the TiO_2 film, but rather from electron doping at the interface. Upon deposition of p-type PbS QDs on top of the encapsulated channel, the threshold voltage clearly shifts back again, indicating a doping compensation effect of the MoS_2/TiO_2 hybrid as a result of the formation of the junction. This leads to dark current in the depletion regime dropping to few tens of pA. In the linear regime,

under a low bias of 100 mV, the two-terminal field-effect mobility was estimated and shows only minor changes at all hybrid stages, ranging from 22–25 cm^2/Vs.

Modulation model.

To understand the effect of the oxide buffer layer, the device characteristics have to be compared with MoS_2/PbS devices where the interface is not protected, referred to as control devices. In Figure 2a typical modulation curves of control devices are plotted before and after sensitization with QDs. The loss of modulation in the control device was associated with strong doping effects, where dithiol ligands initially n-type dope MoS_2 strongly and the addition of p-type PbS reversed the doping effect[13]. Just recently, it was shown that thiols can be used for doping of TMDCs, as the sulfide component chemically interacts with sulfur-vacancy defect sites in the MoS_2 surface[24]. Depending on polarity of the functional group the doping effect can either be p- or n-type. In the case of MoS_2/PbS hybrids, the dithiols fill these defect sites and crosslink to PbS quantum dots, causing a strong charge transfer mechanism. Although doping plays a role upon hybrid formation, it is not the dominant mechanism behind the clear loss of modulation. When the defect-rich MoS_2 surface connects to PbS QDs, a detrimental side-effect of the direct cross-linking is a large density of localized states within the bandgap of the 2D material, as displayed in Figure 2b. As a consequence, the Fermi-level (E_F) is "pinned" and the modulation via backgate voltage is reduced to on/off ratios of 10^2. The pinning effect on FET characteristics is clarified in Figure 2c. Despite the high applied gate voltage, the hybrid device cannot be switched off entirely and considerable amount of current is still induced into the channel. Additionally, the on-current flow in the accumulation regime is clearly reduced compared to its plain MoS_2 counterpart, attributed to the Fermi level pinning below the conduction band edge.

The phenomenon of Fermi-level pinning can be quite problematic in low dimensional semiconductor devices. MoS_2 is known to be prone to such effects at semiconductor-metal interfaces[29,30], where the pinning prevents ohmic contacts to be formed and eventually leads to high contact resistance. Little effort has been made, up to date, to circumvent the pinning effect for metal contacts. A typical method to avoid Fermi-level pinning is to passivate the interface traps with a thin oxide layer. The passivation of the MoS_2 contact area with Al_2O_3[31] or TiO_2 [32] has been demonstrated to produce lower contact resistance.

Figure 2d shows that with a thin TiO_2 film at the MoS_2/PbS interface, low off- and high on-currents close to initial MoS_2 values are obtained in the depletion and accumulation regime, respectively. The regained backgate control over E_F allows efficient channel depletion and accumulation, illustrated schematically in Figure 2e and 2f.

Several devices with protected and unprotected interface have been compared, showing highly reproducible results as summarized in Figure 3. All tested control devices show strongly reduced on/off ratios of only 10^2 with relatively large off currents in the range of 10–100 nA/ μm, at strongest possible gating just before breakdown of the underlying SiO_2. The new device architecture MoS_2/TiO_2/PbS however largely retained its FET properties and the on/off ratio can be improved by more than 2 orders of magnitude compared to control devices. We also note that while the encapsulation improved dramatically the on/off ratio of the devices, we did not observe any effects on the mobility of the MoS_2 channel before and after deposition of the QDs (data are shown in the supporting information, Tables 2 and 3).

Phototransistor properties.

Now we turn to the photodetection performance of the MoS_2/TiO_2/PbS device. In our previous work on MoS_2/PbS devices high gain was found, a mechanism that creates multiple electrons per single absorbed photon. Also, the backgate dependent light response of the

MoS_2/PbS hybrid showed quite peculiar behaviour with a change of sign from positive photoresponse (depletion regime) to negative response (accumulation regime)[13]. The TiO_2 passivation of MoS_2/TiO_2/PbS devices, however, maintains the photoresponse positive throughout the full gate voltage range. Figure 4a demonstrates the modulation curves under dark and illuminated conditions for different illumination power. As depicted in the inset panel, the large bandgap interlayer rules out the possibility of hole injection from PbS into MoS_2 as well as trap-assisted recombination at the interface, both plausible mechanism that might have caused the sign switch of photoresponse in MoS_2/PbS devices.

The photocurrent $I_{PC} = I_{Light} - I_{Dark}$ versus backgate voltage for different illumination intensities (Figure 4b) shows strong modulation with V_G and a clear maximum of response can be identified between 0 V and +5 V. The strongest response corresponds to the region with highest transconductance of the FET device, as observed for standalone MoS_2 detectors[9,33]. The Fermi level alignment in this region is favourable for low contact resistance operation and ideal for many cycles of electron circulation to produce maximum gain. Yet, in this region the hybrid also operates at high dark currents and therefore a more important figure of merit is the signal-to-noise ratio (SNR). In the same panel Figure 4b the SNR defined as I_{PC}/I_{Dark} is illustrated and points out the phototransistors' potential for highest sensitivity in its depletion regime at V_G of -12 V to -15 V. Here the lowest dark currents and a maximum of sensitivity are achieved, despite the devices' concurrent drop in photocurrent.

To investigate in greater detail, we acquired power dependent responsivity defined as $R = I_{PC}/P_{In}$ in the two distinct regimes of operation, at 0 V and -15 V (Figure 5a). At both gate voltages the measured responsivity dropped with increasing power, because of saturation of sensitizing traps in PbS QDs, and shows responsivity of 10^3 A/W and 10^5 A/W at around 10

nW/cm^2. This is a characteristic footprint of trap dominated photoresponse[34,35], where the ratio of longer lifetime of minority carrier ($\tau_{lifetime}$) to short transit time of majority carrier ($\tau_{transit}$) produces internal photoconductive gain, defined as $G = \tau_{lifetime} / \tau_{transit}$.

The decay process can be approximated by a first-order exponential relaxation function (Figure 5b). For a light pulse measured at 67 nW/cm^2 and V_G = -15 V, a time constant τ_{decay} = 12 ms was extracted and with increasing illumination power the device response accelerates. Taking the time constant as a measure of the carrier lifetime, a quantum efficiency of around 28% can be extracted from its responsivity and gain measured at V_G = 0 V (see methods).

The purpose of the TiO_2 interlayer in the MoS_2/TiO_2/PbS hybrid is two-fold, as for one it avoids the creation of high density of trap states at the interface and prevents the pinning of E_F, but also allows charge transport between MoS_2 and PbS. To verify the actual charge transfer mechanism between PbS and MoS_2, the spectral response was measured at V_G = -15 V (Figure 5c). The curve clearly follows the absorption spectrum of the sensitizing QDs with an exciton peak at 965 nm (absorption spectra in SOM Fig. S1). Along with the finding from Figure 5a, it is evident that photons are absorbed within the QD film and charge carriers are subsequently transferred into the MoS_2 channel, where the magnitude of gain can be tuned with FET channel conductance.

To assess the sensitivity of MoS_2/TiO_2/PbS hybrid devices, the noise spectral density was measured at both gate voltages and spectral detectivity at 1 Hz bandwidth was calculated with $D^*(\lambda, 1\text{Hz}) = R \times (AB)^{1/2} / i_N$, where A is the active detector area, B the bandwidth and i_N the noise current (see SOM S2 for details). In the earlier predicted, highest SNR regime at around -15 V, the hybrid device reaches specific detectivity 5×10^{12} Jones in the visible and exceeds 10^{12} Jones throughout the NIR wavelength range, measured at low applied electric fields of only 0.2 V/µm (Figure 5c). In the depletion regime the measured noise reaches the limit of

the measurement system and even higher sensitivities can be expected for this device design. The shot-noise estimated detectivity of 3×10^{14} Jones showcases the potential of the new device architecture with further room of improvement. The dominant 1/f noise component and the fast response point to higher sensitivity at higher frequencies. In the highly responsive regime, at $V_G = 0$ V, the sensitivity D^* reduces as expected to 3×10^{11} Jones due to its larger dark and noise current.

Discussion

To summarize, we successfully incorporated a thin oxide buffer layer at the heterojunction of a 2D-dichalcogenide and an absorbing sensitizer. In a proof-of-concept device, consisting of a MoS_2 - PbS QDs hybrid phototransistor, we passivated present defect sites at the interface with a thin semiconducting TiO_2 layer and thereby retain electrical control of its FET characteristics. The interlayer avoids the formation of a high density of localized states in the sub-bandgap region that pin the Fermi level and hamper significantly its current modulation, as it is the case for unprotected MoS_2/PbS devices. With this passivation scheme we achieved an improvement in modulation by more than 2 orders of magnitude, close to initial MoS_2 on/off-ratios. Moreover, the buffer layer at the junction serves as efficient charge separation and transport layer leading to quantum efficiency of 28%. The demonstrated phototransistors show excellent performance parameters with detectivity of 5×10^{12} Jones in the visible and temporal response of $\leq$ 12 ms, more than an order of magnitude improvement in sensitivity and speed compared to control devices[13]. We have presented a new route to engineer the interface between 2D materials and strong absorbing semiconductors to form efficient heterojunctions without losing its unique electrical properties. We anticipate that this passivation

mechanism creates a new path to better control interface and doping effects of 2D-crystal-based heterostructures and can be useful for a wide range of applications.

Methods

MoS_2 FET fabrication

MoS_2 flakes of different thickness (1–10 layers) were exfoliated with PDMS tape on pre-cleaned Si/SiO_2 (90 nm) wafer. Metal contacts were fabricated by means of direct laser writer lithography and Ti (2 nm) and Au (80 nm) electrodes were evaporated by e-beam and thermal evaporation, respectively. The final devices were annealed for 2h in ultrahigh vacuum at 150ºC to improve contact resistance. Residual metal was lifted-off in NMP (1-methyl-2-pyrrolidone) for 2h, followed by thorough Acetone and Isopropanol rinse. Inspection and structural characterization of the MoS_2 devices considered in this work are provided in Fig. S4 of the supporting information, including optical microscopy images and Raman characterization.

PbS QD film deposition

The synthesis of PbS quantum dots was carried out under inert conditions using a Schlenk line as described in previous work[13]. The PbS thin film was spincoated in a standard layer-by-layer approach at rotation speed of 2000 rpm. The QD concentration used was 30 mg/ml in toluene and EDT solution for ligand exchange was 2 vol. % in Acetonitrile. Toluene and Acetonitrile were used to rinse the device after each layer of QDs and EDT deposition. The resulting thickness of reported samples was in the range of 80–100 nm.

TiO_2 ALD deposition

After test measurements in ambient conditions, devices were covered by TiO_2 with atomic layer deposition technique (Savannah 200, Cambridge Nanotech). Prior to deposition, samples were annealed in nitrogen atmosphere in the ALD chamber at 200ºC for around 1h to remove surface bound adsorbates. The carrier and purge gas of the entire process was nitrogen. The temperature during the deposition process was maintained at 200 ºC. Titanium isopropoxide and H_2O precursors were used alternating with open valve times of 0.1 s and 0.015 s, respectively, separated by a 10 s pump time. The resulting growth rate was determined with a profilometer (Alpha-Step IQ) to be 0.04 nm/cycle.

Electrical characterization

All Current-voltage measurements were performed in ambient conditions using an Agilent B1500A semiconducting device analyser. The light response was recorded under global illumination with a spot size of 2 mm. For spectral photoresponse measurements the devices were illuminated with fiber-coupled and spectrally filtered light from a supercontinuum light source (SuperKExtreme EXW-4, NKT Photonics). Responsivity and temporal response times were measured under short-pulsed light at a wavelength of 635nm from a 4-channel LASER controlled with an Agilent A33220A waveform generator.

The frequency dependent noise current was obtained by analysing the dark current in the conducting channel. Several dark current traces were acquired with the Agilent system under same V_G and V_{DS} conditions as the optical measurements. Since responsivity was measured at light modulation frequency of 1 Hz, the noise current was extracted at 1 Hz to calculate the corresponding detectivity D^*(1Hz). The frequency dependent noise spectral density at two different V_G and the estimation of D^* at higher frequency can be found in the supplementary information.

Quantum efficiency estimation

The quantum efficiency *QE* of the hybrid phototransistors can be calculated from the measured responsivity *R* and an estimation of the photoconductive gain *G*, by using:

$$R = \frac{\lambda e}{hc} \times QE \times G \qquad with \qquad G = \frac{\tau_{lifetime}}{\tau_{transit}}$$

where λ is the wavelength, *e* the elementary charge, *h* is the Planck constant, *c* the speed of light, and the photoconductive gain *G* is given by the ratio of carrier lifetime $\tau_{lifetime}$ over the transit time $\tau_{transit}$. The lifetime corresponds to the time constant of the photoresponse. The transit time, the time electrons need to flow through the MoS_2 channel from source to drain, is given by $L^2/\mu V_{DS}$, with *L* the channel length, μ the carrier mobility and V_{DS} the source-drain voltage. As the gain is strongly influenced by the applied gate voltage, we extracted the necessary data from measurements at $V_G = 0$ V (SOM Fig. S3), where the FET is operated in accumulation and contacts are rather ohmic (as explained in the manuscript). With a transit time of 4.7 ns, this results in a photoconductive gain of 1.7×10^6 and finally in a $QE \sim 28\%$.

Supporting Information:

TiO_2 thickness dependence (T1), PbS absorption spectrum (S1), Noise spectra and detectivity estimation (S2), Decay time estimation (S3), Mobility before and after PbS deposition (T2, T3), Microscope images and Raman spectra (S4).

Acknowledgments:

We acknowledge funding support from European Commission's Seventh Framework Programme under Graphene Flagship (contract no. CNECT-ICT-604391) and Fundació Privada Cellex Barcelona. We are also thankful to the Ministerio de Ciencia e Innovación under contract number TEC2011-24744 for financial support. D.K. is supported by an FI fellowship. We acknowledge financial support from the Spanish Ministry of Economy and Competitiveness, through the "Severo Ochoa" Programme for Centres of Excellence in R&D (SEV-2015-0522). FK acknowledges support by the ERC starting grant (307806, CarbonLight), the Government of Catalonia trough the SGR grant (2014-SGR-1535), the Mineco grants Ramón y

Cajal (RYC-2012-12281) and Plan Nacional (FIS2013-47161-P).

(1) Koppens, F. H. L.; Mueller, T.; Avouris, P.; Ferrari, A. C.; Vitiello, M. S.; Polini, M. Photodetectors based on graphene, other two-dimensional materials and hybrid systems. *Nat. Nanotechnol.* **2014**, *9*, 780–793.

(2) Konstantatos, G.; Badioli, M.; Gaudreau, L.; Osmond, J.; Bernechea, M.; Garcia de Arquer, F. P.; Gatti, F.; Koppens, F. H. L. Hybrid graphene-quantum dot phototransistors with ultrahigh gain. *Nat. Nanotechnol.* **2012**, *7*, 363–368.

(3) Sun, Z.; Liu, Z.; Li, J.; Tai, G.-A.; Lau, S.-P.; Yan, F. Infrared photodetectors based on CVD-grown graphene and PbS quantum dots with ultrahigh responsivity. *Adv. Mater.* **2012**, *24*, 5878–5883.

(4) Manga, K. K.; Zhou, Y.; Yan, Y.; Loh, K. P. Multilayer hybrid films consisting of alternating graphene and titania nanosheets with ultrafast electron transfer and photoconversion properties. *Adv. Funct. Mater.* **2009**, *19*, 3638–3643.

(5) Lee, Y.; Kwon, J.; Hwang, E.; Ra, C.-H.; Yoo, W. J.; Ahn, J.-H.; Park, J. H.; Cho, J. H. High-performance perovskite-graphene hybrid photodetector. *Adv. Mater.* **2015**, *27*, 41–46.

(6) Roy, K.; Padmanabhan, M.; Goswami, S.; Sai, T. P.; Ramalingam, G.; Raghavan, S.; Ghosh, A. Graphene-MoS_2 hybrid structures for multifunctional photoresponsive memory devices. *Nat. Nanotechnol.* **2013**, *8*, 826–830.

(7) Zhang, W.; Chuu, C.-P.; Huang, J.-K.; Chen, C.-H.; Tsai, M.-L.; Chang, Y.-H.; Liang, C.-T.; Chen, Y.-Z.; Chueh, Y.-L.; He, J.-H.; Chou, M.-Y.; Li, L.-J. Ultrahigh-gain

photodetectors based on atomically thin graphene-MoS_2 heterostructures. *Sci. Rep.* **2014**, *4*, 3826.

(8) Choi, W.; Cho, M. Y.; Konar, A.; Lee, J. H.; Cha, G.-B.; Hong, S. C.; Kim, S.; Kim, J.; Jena, D.; Joo, J.; Kim, S. High-detectivity multilayer MoS_2 phototransistors with spectral response from ultraviolet to infrared. *Adv. Mater.* **2012**, *24*, 5832–5836.

(9) Kufer, D.; Konstantatos, G. Highly Sensitive, Encapsulated MoS_2 Photodetector with Gate Controllable Gain and Speed. *Nano Lett.* **2015**, *15*, 7307–7313.

(10) Lopez-Sanchez, O.; Lembke, D.; Kayci, M.; Radenovic, A.; Kis, A. Ultrasensitive photodetectors based on monolayer MoS_2. *Nat. Nanotechnol.* **2013**, *8*, 497–501.

(11) Furchi, M. M.; Polyushkin, D. K.; Pospischil, A.; Mueller, T. Mechanisms of Photoconductivity in Atomically Thin MoS_2. *Nano Lett.* **2014**, *14*, 6165–6170.

(12) Zhang, W.; Huang, J.-K.; Chen, C.-H.; Chang, Y.-H.; Cheng, Y.-J.; Li, L.-J. High-Gain Phototransistors Based on a CVD MoS_2 Monolayer. *Adv. Mater.* **2013**, *25*, 3456–3461.

(13) Kufer, D.; Nikitskiy, I.; Lasanta, T.; Navickaite, G.; Koppens, F. H. L.; Konstantatos, G. Hybrid 2D–0D MoS_2–PbS Quantum Dot Photodetectors. *Adv. Mater.* **2015**, *27*, 176–180.

(14) Lin, J. D.; Han, C.; Wang, F.; Wang, R.; Xiang, D.; Qin, S.; Zhang, X.-A.; Wang, L.; Zhang, H.; Wee, A. T. S.; Chen, W. Electron-Doping-Enhanced Trion Formation in Monolayer Molybdenum Disulfide Functionalized with Cesium Carbonate. *ACS Nano* **2014**, *8*, 5323–5329.

(15) Kiriya, D.; Tosun, M.; Zhao, P.; Kang, J. S.; Javey, A. Air-Stable Surface Charge Transfer Doping of MoS_2 by Benzyl Viologen. *J. Am. Chem. Soc.* **2014**, *136*, 7853–7856.

(16) Fang, H.; Tosun, M.; Seol, G.; Chang, T. C.; Takei, K.; Guo, J.; Javey, A. Degenerate

n-Doping of Few-Layer Transition Metal Dichalcogenides by Potassium. *Nano Lett.* **2013**, *13*, 1991–1995.

(17) Yang, L.; Majumdar, K.; Liu, H.; Du, Y.; Wu, H.; Hatzistergos, M.; Hung, P. Y.; Tieckelmann, R.; Tsai, W.; Hobbs, C.; Ye, P. D. Chloride Molecular Doping Technique on 2D Materials: WS_2 and MoS_2. *Nano Lett.* **2014**, *14*, 6275–6280.

(18) Du, Y.; Liu, H.; Neal, A. T.; Si, M.; Ye, P. D. Molecular Doping of Multilayer MoS_2 Field-Effect Transistors: Reduction in Sheet and Contact Resistances. *IEEE Electron Device Lett.* **2013**, *34*, 1328–1330.

(19) Suh, J.; Park, T.-E.; Lin, D.-Y.; Fu, D.; Park, J.; Jung, H. J.; Chen, Y.; Ko, C.; Jang, C.; Sun, Y.; Sinclair, R.; Chang, J.; Tongay, S.; Wu, J. Doping against the Native Propensity of MoS_2: Degenerate Hole Doping by Cation Substitution. *Nano Lett.* **2014**, *14*, 6976–6982.

(20) Zhang, K.; Feng, S.; Wang, J.; Azcatl, A.; Lu, N.; Addou, R.; Wang, N.; Zhou, C.; Lerach, J.; Bojan, V.; Kim, M. J.; Chen, L.-Q.; Wallace, R. M.; Terrones, M.; Zhu, J.; Robinson, J. A. Manganese Doping of Monolayer MoS_2: The Substrate Is Critical. *Nano Lett.* **2015**, *15*, 6586–6591.

(21) Mouri, S.; Miyauchi, Y.; Matsuda, K. Tunable Photoluminescence of Monolayer MoS_2 via Chemical Doping. *Nano Lett.* **2013**, *13*, 5944–5948.

(22) Lei, S.; Wang, X.; Li, B.; Kang, J.; He, Y.; George, A.; Ge, L.; Gong, Y.; Dong, P.; Jin, Z.; Brunetto, G.; Chen, W.; Lin, Z.-T.; Baines, R.; Galvão, D. S.; Lou, J.; Barrera, E.; Banerjee, K.; Vajtai, R.; Ajayan, P. Surface functionalization of two-dimensional metal chalcogenides by Lewis acid–base chemistry. *Nat. Nanotechnol.* **2016**, *advance on*.

(23) Yu, Z.; Pan, Y.; Shen, Y.; Wang, Z.; Ong, Z.-Y.; Xu, T.; Xin, R.; Pan, L.; Wang, B.; Sun, L.; Wang, J.; Zhang, G.; Zhang, Y. W.; Shi, Y.; Wang, X. Towards intrinsic

charge transport in monolayer molybdenum disulfide by defect and interface engineering. *Nat. Commun.* **2014**, *5*, 5290.

(24) Sim, D. M.; Kim, M.; Yim, S.; Choi, M.-J.; Choi, J.; Yoo, S.; Jung, Y. S. Controlled Doping of Vacancy-Containing Few-Layer MoS_2 *via* Highly Stable Thiol-Based Molecular Chemisorption. *ACS Nano* **2015**, *9*, 12115–12123.

(25) Li, S.-L.; Komatsu, K.; Nakaharai, S.; Lin, Y.-F.; Yamamoto, M.; Duan, X.; Tsukagoshi, K. Thickness Scaling Effect on Interfacial Barrier and Electrical Contact to Two-Dimensional MoS_2 Layers. *ACS Nano* **2014**, *8*, 12836–12842.

(26) Barkhouse, D. A. R.; Debnath, R.; Kramer, I. J.; Zhitomirsky, D.; Pattantyus-Abraham, A. G.; Levina, L.; Etgar, L.; Grätzel, M.; Sargent, E. H. Depleted Bulk Heterojunction Colloidal Quantum Dot Photovoltaics. *Adv. Mater.* **2011**, *23*, 3134–3138.

(27) Carey, G. H.; Abdelhady, A. L.; Ning, Z.; Thon, S. M.; Bakr, O. M.; Sargent, E. H. Colloidal Quantum Dot Solar Cells. *Chem. Rev.* **2015**, *115*, 12732–12763.

(28) Pattantyus-Abraham, A. G.; Kramer, I. J.; Barkhouse, A. R.; Wang, X.; Konstantatos, G.; Debnath, R.; Levina, L.; Raabe, I.; Nazeeruddin, M. K.; Grätzel, M.; Sargent, E. H. Depleted-Heterojunction Colloidal Quantum Dot Solar Cells. *ACS Nano* **2010**, *4*, 3374–3380.

(29) Gong, C.; Colombo, L.; Wallace, R. M.; Cho, K. The Unusual Mechanism of Partial Fermi Level Pinning at Metal–MoS_2 Interfaces. *Nano Lett.* **2014**, *14*, 1714–1720.

(30) Das, S.; Chen, H.-Y.; Penumatcha, A. V.; Appenzeller, J. High Performance Multilayer MoS_2 Transistors with Scandium Contacts. *Nano Lett.* **2013**, *13*, 100–105.

(31) Park, W.; Kim, Y.; Jung, U.; Cho, C.; Lee, H.-B.-R. Contact resistance reduction using Fermi level de-pinning layer for MoS_2 FETs. In *2014 IEEE International Electron Devices Meeting*; IEEE, 2014; pp. 5.1.1–5.1.4.

(32) Kaushik, N.; Karmakar, D.; Nipane, A.; Karande, S.; Lodha, S. Interfacial n-Doping Using an Ultrathin TiO_2 Layer for Contact Resistance Reduction in MoS_2. *ACS Appl. Mater. Interfaces* **2016**, *8*, 256–263.

(33) Li, H.-M.; Lee, D.-Y.; Choi, M. S.; Qu, D.; Liu, X.; Ra, C.-H.; Yoo, W. J. Metal-Semiconductor Barrier Modulation for High Photoresponse in Transition Metal Dichalcogenide Field Effect Transistors. *Sci. Rep.* **2014**, *4*, 4041.

(34) Konstantatos, G.; Sargent, E. H. Solution-Processed Quantum Dot Photodetectors. *Proc. IEEE* **2009**, *97*, 1666–1683.

(35) Konstantatos, G.; Clifford, J.; Levina, L.; Sargent, E. H. Sensitive solution-processed visible-wavelength photodetectors. *Nat. Photonics* **2007**, *1*, 531–534.

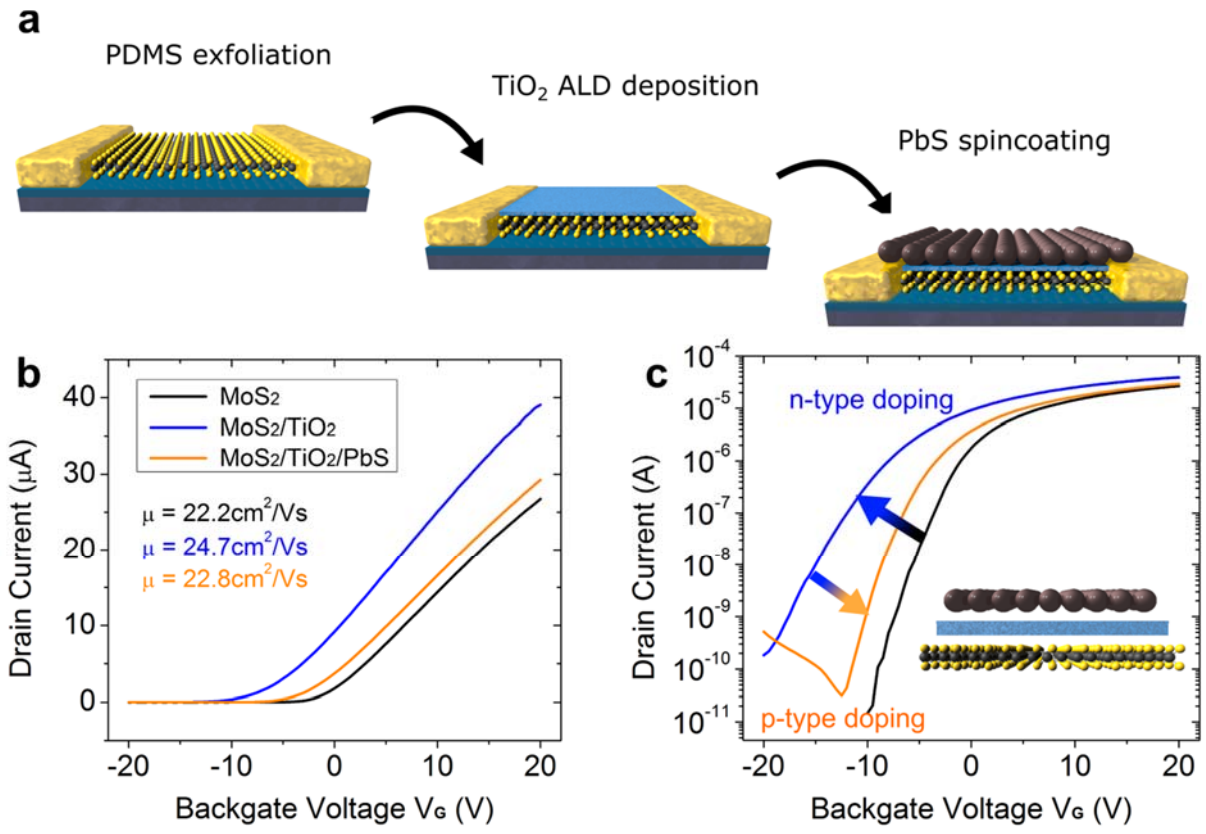

Figure 1. Device design and FET properties. (a) Device architecture after each fabrication step. Few-layer MoS_2-FETs are fabricated by PDMS tape exfoliation and standard lithography, the TiO_2 film is deposited by atomic layer deposition, and colloidal quantum dots are spincoated in a layer-by-layer process. The transfer curves for all stages of fabrication are plotted in linear (b) and logarithmic (c) scale. The shift of threshold voltage indicates clear n-type and p-type doping after TiO_2 and PbS deposition, respectively. V_{DS} = 1V.

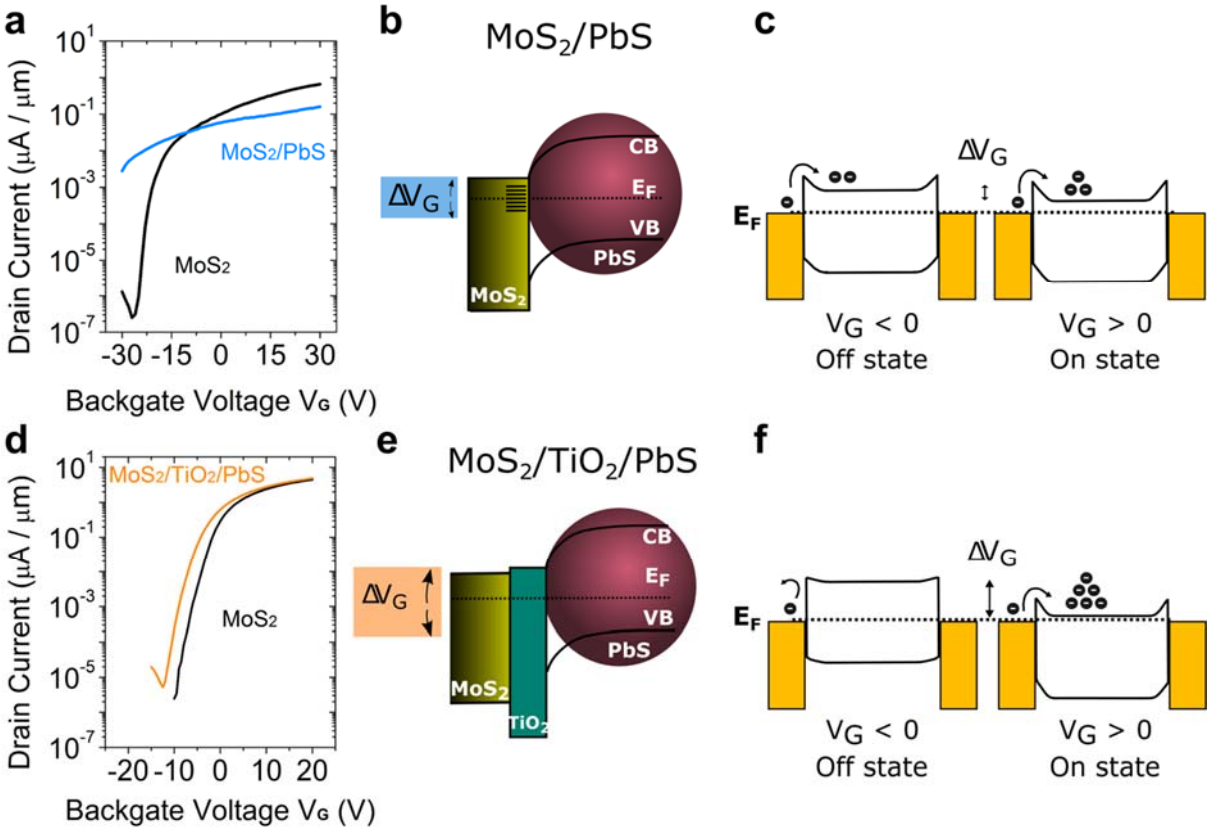

Figure 2. Modulation model. (a) Transfer curve of a typical MoS_2/PbS control device. The on/off ratio of the standalone MoS_2 device is strongly reduced after PbS deposition. (b) Band alignment of MoS_2 and PbS in direct contact. The crosslinking with dithiol ligands creates high density of localized sub-bandgap states in MoS_2 that pins E_F and reduces gate tunability to a small range ΔV_G. (c) Band diagram of the MoS_2 channel after PbS deposition with Schottky-barrier at the contact regions. The FET channel can neither be sufficiently switched off (off state) nor fully turned on (on state) due to the reduced E_F control by backgate voltage. Panel (d) – (f) show the same model for the case of interface protected MoS_2/TiO_2/PbS hy-

brids. The on/off ratio is now widely maintained (d) because of an effective passivation of the interface region (e). The control of E_F is preserved leading to low off state current injection and high on state current flow (f).

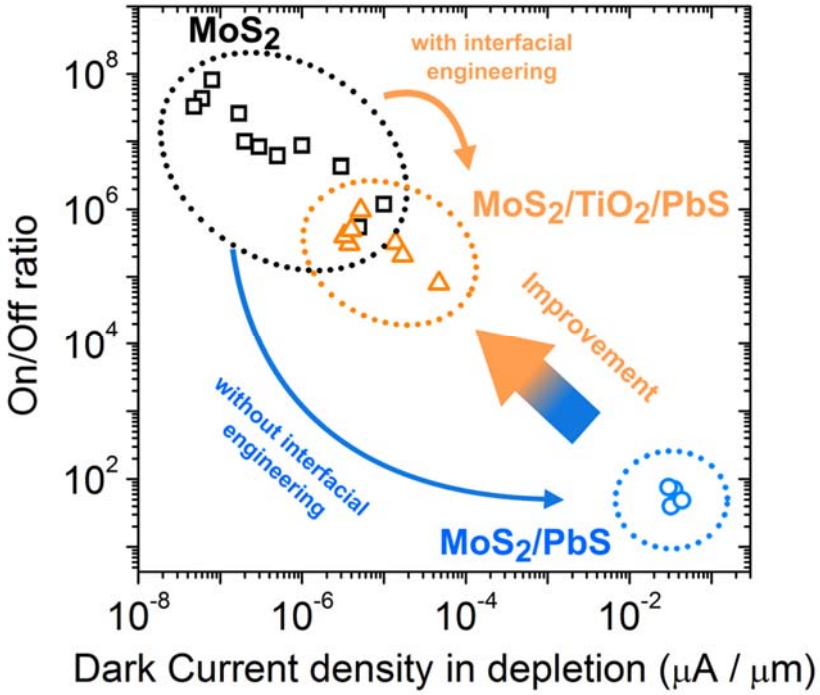

Figure 3. Transistor operation improvement after interface engineering. On/off ratio versus dark current density, plotted for many tested devices with similar channel dimensions in their depletion regime. Initially obtained ratios of 10^6-10^8 for standalone MoS_2 are strongly reduced to 10^2 for MoS_2/PbS control devices (blue arrow) and only slightly decreased to 10^5-10^6 for interlayer protected MoS_2/TiO_2/PbS devices (orange arrow). Likewise, dark currents are strikingly decreased by more than 3 orders of magnitude after implementation of the buffer layer.

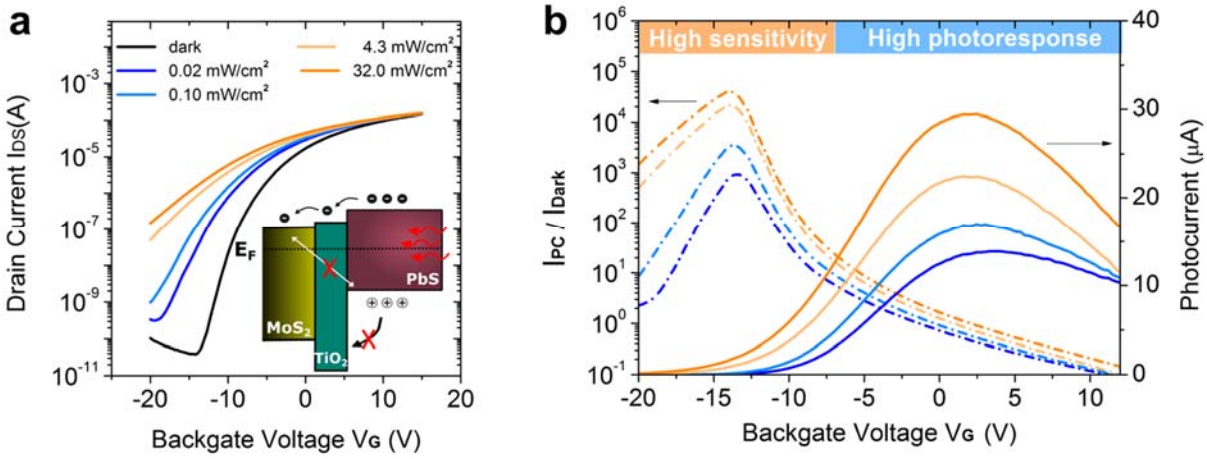

Figure 4. Backgate dependent photoresponse and sensitivity. (a) Transfer curves of a hybrid $MoS_2/TiO_2/PbS$ device at different illumination intensity specified in the legend. The small inset illustrates the electron charge transfer mechanism after photoexcitation due to well aligned conduction bands. Holes stay trapped in the PbS film as they can neither surpass the large TiO_2 barrier nor recombine with electrons in the MoS_2 channel. (b) Backgate dependent photocurrent (right axis) and SNR ratio defined as ratio of photocurrent and dark current (left axis). Despite the strongest light response above the threshold voltage ($V_G \sim 0V$), the highest sensitivity of the device is reached in the depletion regime ($V_G \sim -15V$).

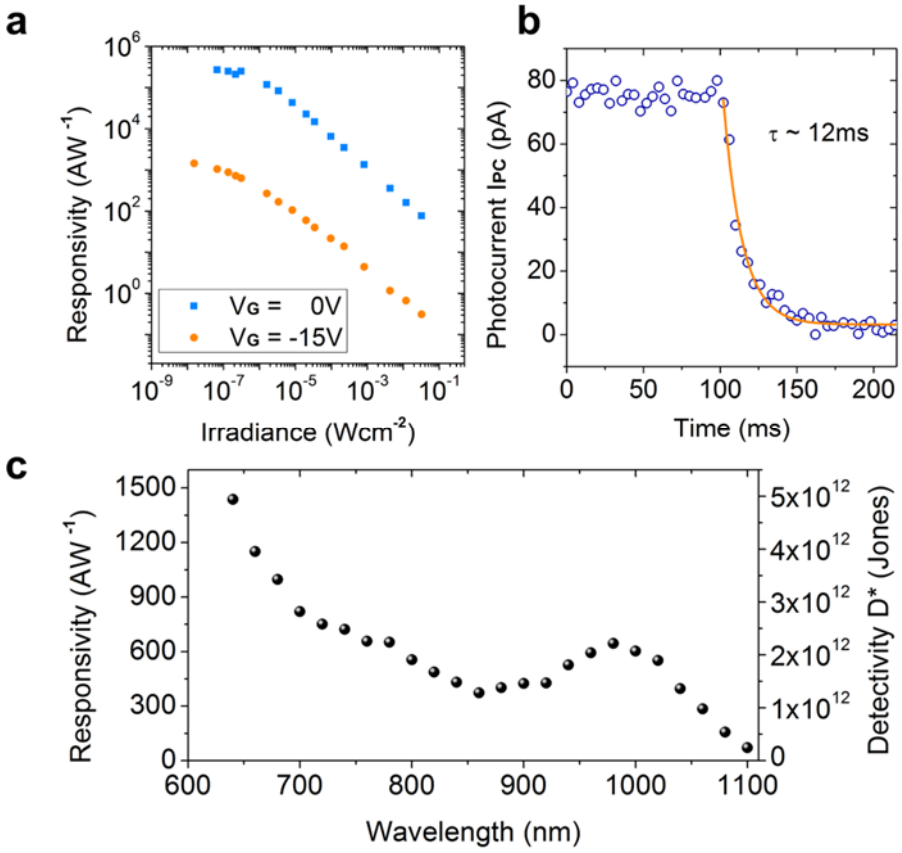

Figure 5. $MoS_2/TiO_2/PbS$ phototransistor properties. (a) Power dependent responsivity measured in the highly sensitive (-15 V) and highly responsive (0 V) regime. V_{DS} =1 V. (b) Decay time of a light response at 67 nW/cm^2. The approximation with a single exponential function results in a time constant of 12 ms. (c) Spectral responsivity (left axis) and detectivity (right axis) reveal a highly sensitive hybrid system with light absorption in the quantum dot thin film. The sensitivity of the hybrid system exceeds 10^{12} Jones over the whole vis/NIR spectral range.

For table of contents use only:

Interface Engineering in hybrid Quantum Dot – 2D phototransistors

Dominik Kufer, Tania Lasanta, Maria Bernechea, Frank Koppens and Gerasimos Konstantatos

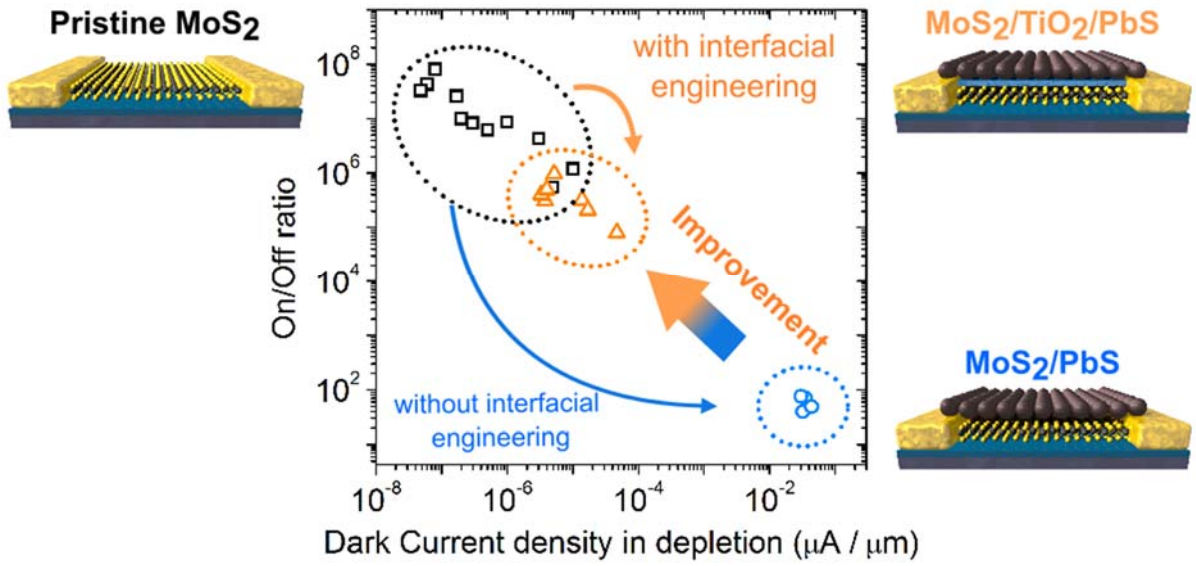

The hybridization of two-dimensional transition metal dichalcogenides (TMDCs) with colloidal quantum dots is demonstrated to be an ideal platform for highly sensitive photodetection. The interface of TMDC-QD hybrids and controlled doping is thereby of paramount importance for low noise operation. To maintain the unique electrical field-effect modulation in TMDCs upon deposition of colloidal quantum dots, a passivation route of the interface with semiconducting metal-oxide films is developed. The retained field-effect modulation with a large on/off ratio allows operation of the phototransistor at significantly lower dark currents than non-passivated hybrids improving its sensitivity. The present passivation method discloses a new path to control interface and degenerate doping effects of 2D-crystal-based hybrid devices and can be useful for a wide range of applications.